1-1-2016

# Influence of Cr-Rich oxide scale on sliding wear mechanism of ferritic stainless steel at high temperature

Xiawei Cheng
*University of Wollongong*, xiawei@uow.edu.au

Zhengyi Jiang
*University of Wollongong*, jiang@uow.edu.au

Buyung Kosasih
*University of Wollongong*, buyung@uow.edu.au

Hui Wu
*University of Wollongong*, hw944@uowmail.edu.au

Suzhen Luo
*Baoshan Iron and Steel Co., Ltd.*

*See next page for additional authors*

# Influence of Cr-Rich oxide scale on sliding wear mechanism of ferritic stainless steel at high temperature


## Abstract

The tribological tests of a ferritic stainless steel (FSS) 445 in contact with high-speed steel (HSS) were performed on a high-temperature pin-on-disc tribometer. Wear exhibited significant difference when the FSS 445 was oxidised with a Cr-rich oxide scale on the surface. The HSS pin displayed adhesive wear when there was no oxide scale on the stainless steel disc, and in the early stages, the coefficient of friction fluctuated significantly, but the level of wear changed as Cr2O3 particles formed. The wear was then reduced, and the coefficient of friction remained stable. The Cr-rich oxide scale which formed on the stainless steel was able to stabilise the coefficient of friction, to reduce the wear rate and to help form a glazed layer on the HSS surface. The abrasive wear of the HSS pin took place at 850 °C, indicating that the hardness of the Cr-rich oxide scale increased as the temperature decreased.



## Keywords

steel, stainless, ferritic, mechanism, wear, high, sliding, influence, scale, oxide, rich, cr, temperature


## Disciplines

Engineering | Science and Technology Studies


## Publication Details

Cheng, X., Jiang, Z., Kosasih, B., Wu, H., Luo, S. & Jiang, L. (2016). Influence of Cr-Rich oxide scale on sliding wear mechanism of ferritic stainless steel at high temperature. Tribology Letters, 63 (2), 1-13.



## Authors

Xiawei Cheng, Zhengyi Jiang, Buyung Kosasih, Hui Wu, Suzhen Luo, and Laizhu Jiang

# Influence of Cr-rich oxide scale on sliding wear mechanism of ferritic stainless steel at high temperature

Xiawei Cheng[1], Zhengyi Jiang[1,*], Buyung Kosasih[1], Hui Wu [1], Suzhen Luo[2], Laizhu Jiang[2]

[1]School of Mechanical, Materials and Mechatronic Engineering, University of Wollongong, NSW 2522, Australia
[2]Baosteel Research Institute (R&D Centre), Baoshan Iron & Steel Co., Ltd., Shanghai 200431, PR China

## Abstract

The tribological tests of a ferritic stainless steel (FSS) 445 in contact with high speed steel (HSS) were performed on a high temperature pin-on-disc tribometer. Wear exhibited significant difference when the FSS 445 was oxidised with a Cr-rich oxide scale on the surface. The HSS pin displayed adhesive wear when there was no oxide scale on the stainless steel disc and in the early stages, the coefficient of friction fluctuated significantly but the level of wear changed as $Cr_2O_3$ particles formed. The wear was then reduced and the coefficient of friction remained stable. The Cr-rich oxide scale which formed on the stainless steel was able to stabilize the coefficient of friction, to reduce the wear rate and to help form a glazed layer on the HSS surface. The abrasive wear of the HSS pin took place at 850 °C, indicating that the hardness of the Cr-rich oxide scale increased as the temperature decreased.

**Keywords:** Ferrous Alloys, Steel; Oxides; EDS; SEM

* Corresponding author: Tel: 61 2 4221 4545; Fax: 61 2 42215474;
E-mail addresses: xiawei@uow.edu.au (X. Cheng); jiang@uow.edu.au (Z. Jiang)

## 1. Introduction

It is known that during the hot working of carbon steel, Wüstite (FeO) has low hardness at high temperatures and acts as a lubricant reducing the wear rate and coefficient of friction. Magnetite ($Fe_3O_4$) has an intermediate hardness and also plays a lubricant role, whereas hematite ($\alpha$-$Fe_2O_3$) has a high hardness that promotes abrasive wear [1,2]. The oxide scale on stainless steels, however, exhibits complicated characteristics because the oxidation is significantly affected by the alloying elements and the atmosphere [3]. The two major phases of a stainless steel oxide scale are the $M_2O_3$ rhombohedral phase and the $M_3O_4$ spinel phase [4-7].

Compared to carbon steels, stainless steels have higher oxidation resistance due to their Cr content. Cr is the main element used in order to induce corrosion resistance in stainless steels. Generally, the higher the Cr concentration, the higher the oxidation resistance is [8]. For instance, on a ferritic stainless steel grade 445, breakaway oxidation does not take place at 1120 °C in a reheating environment [5] and this indicates that the oxide scale is thin because the thick non-protective iron-rich oxide scale has not formed . The oxide scale may have different tribological behaviour and differing relative thicknesses depending on the temperature [9], the atmosphere, and the chemical composition of the alloys [10]. The surface oxide layer of steel can change the tribological characteristics of lubrication [11]. The oxide scale could be abrasive or lubricated. Oxide debris, if it is hard and brittle, may act as free third bodies abrading the antagonistic surfaces [12]. On the other hand, oxide scale may also decrease metal-on-metal contact during the relative sliding motion of the metallic parts, thus protecting them against wear [13]. Some

researchers [14-19] have found that the oxides, whether they were generated during the sliding test or introduced by external methods, may form a tribofilm on steel surfaces which rub together.

The oxide scale plays an important role in the sticking mechanisms during the hot rolling of ferritic stainless steels [20-24] but the tribological behaviour of the oxide scale formed on the stainless steel 445 has not been investigated. Pin-on-disc experiments were conducted at elevated temperature. Because the oxide scale on the 445 stainless steel is barely formed when the temperature is below 1000 °C [5], by considering the maximum operating temperature of 1000 °C for the CETR UMT Multi-specimen Test System, pre-oxidation of the steel 445 is needed in order to obtain a thickening of the oxide scale in the experiment.

## 2. Experimental details

Tribological tests were carried out under a pin-on-disc configuration on a CETR tribometer as shown in Fig. 1. This device is not a hot rolling simulator as there was only continuously sliding contact, which is different from the rolling contact in actual rolling practice but the contact mechanics can be established between the grade of the hot working roll (pin) and the hot strip material (disc) [25].

The chemical compositions of these two materials are listed in Tables 1 and 2, respectively. The hardness of the HSS (pin) was 835±35 HV and the hardness of the ferritic stainless steel 445

(disc) was 172±9 HV at room temperature. The pin was formed into a mushroom shape with a 5 mm radius flat end as shown in Fig. 1.

The disc was heated up to the set temperature in a heating chamber and was kept rotating in order to distribute the heat uniformly in the chamber, while the pin was kept 5 mm away from the disc. A K-type thermocouple was placed underneath the disc to monitor its temperature during the tribological test. When the temperature of the disc reached the set temperature and allowed to stabilize, for a total of 130 min, the pin was brought into contact with the rotating disc under the set force. The duration of the test was 30 min. After each test, the pin was lifted to 5 mm away from the disc and cooled slowly in the chamber, in order to eliminate any spallation of the oxide scale caused by the a sudden temperature change.

The clean surface of the ferritic stainless steel 445 disc was polished to a roughness Ra of 1 μm and cleaned with ethanol before testing. The oxidised surface of the steel 445 was obtained by placing the discs in an electric furnace at 1100 °C for 120 min and then slowly cooled down to room temperature. In this way, the thickness of the oxide scale on all the oxidised discs was kept the same. The HSS pin was machined to a roughness Ra of 2.5 μm. A constant load of 30 N was applied to press the high-speed steel pin against the rotating disc plate for a period of 30 min. The angular velocity and the diameter of the wear track were 34 rpm and 14 mm, respectively, corresponding to a total linear sliding distance of 90 m. In order to verify the results, two identical tests were carried out. The friction curves in both experiments were identical. During each test, variations of the coefficient of friction were recorded as a function of the sliding time.

X-ray diffractometer (XRD), a KEYENCE 3D laser-scanning microscope and a JEOL JSM-6490 type scanning electron microscope (SEM) equipped with an energy dispersion spectrometer (EDS) were used to characterize the structure, morphology, and composition of the worn surface, its longitudinal cross-section, and the wear debris collected after the wear test.

## 3. Results

### 3.1. Microstructures of the Cr-rich oxide scale

Fig. 2a-c shows the micrograph, the XRD patterns and the cross section of the oxide scale formed on the surface of the steel 445 oxidised at 1100 ºC for 120 min before wear tests. The features of the oxide scale are similar to our previous study [23] due to the same oxidation process. Fig. 2a shows the surface morphology of the oxide scale. Some coarse tetrahedral spinel crystallites are embedded in the fine chromia scale matrix.

The oxide scale constituted of $Cr_2O_3$. $Cr_2O_3$ has a corundum structure, which consists of an hcp array of oxygen with two-thirds of the octahedral sites occupied by the metal [26-28]. $(Mn,Cr)_3O_4$ Spinel is located on top of $Cr_2O_3$ scale. Si segregates at the interface of metal-oxide scale where the black islands underneath the $Cr_2O_3$ are. The oxide scale thickness is 6.1±0.23 μm. Mn content in the oxide layers was found to coexist with the Cr oxide, demonstrating that Mn has a higher affinity to oxygen than iron and a greater diffusivity through the Cr oxide [4]. For the oxides formed on the steel 445, Mn was rich at the gas-scale interface, and spinel

$(Mn,Cr)_3O_4$ was detected. The formation of Mn-Cr oxide can reduce Cr activity, and Mn-Cr oxides are known to provide protection against oxidation [26-29].

Rockwell hardness testing was used to measure the hardness of the oxidised disc. The indenter is a hard steel ball with 1/16 inch diameter. Ten measurements were done on clean and oxidised discs and the Rockwell B HRB values were 84.8±0.6 and 84.0±1.0, respectively. Fig. 3 shows indents on clean and oxidised ferrtic stainless steel 445 at a load of 100 kgf. The diameter and the depth of the indents are similar; indicating not much change of the substrate hardness after the oxide scale was formed during the oxidation process.

### 3.2. Friction and wear behaviour

It should be noted that the pins were located 5 mm away from the rotating disc. Oxidation barely took place on the pins at this distance and after this short time. For this reason, it was assumed that there was no oxide scale formed on the HSS pins before the pin was brought into contact against the disc. Fig. 4 shows the coefficient of friction (COF) and the HSS pin displacement as a function of sliding time for the clean discs siding against the HSS pins at 850 and 950 °C. In this case, the initial contact was considered as a metallic pin on a metallic disc.

Fig. 4a shows the curves of COF that can be divided into two stages; (i) the first stage, noted Stage I, corresponding to the start of the friction curve. The curves show big fluctuation at this stage, but a decreasing tendency; (ii) the second stage, noted Stage II, corresponding to the

stabilisation step of COF. It can be seen from the insert in Fig. 4a, at 950 °C, the duration of Stage I is 760 sec, while at 850 °C, the duration of Stage I is 950 sec, and eventually a steady value is attained for the rest of the operation. It took longer to reach stabilized Stage II when the test temperature was lower. In order to understand the fluctuated frictional behaviour in Stage I, a tribological test was interrupted at the test time of 480 sec at 850 °C, and this will be discussed later.

Fig. 4b shows the pin displacement curves. The curves can provide information on *in situ* contact of the counterparts. They have the same tendency as that of the curves of COF. The pin fluctuated greatly at 850 °C, indicating that the wear of the steel 445 disc is uneven and severe during Stage I. The curve of the pin displacement reaches a relatively steady state in Stage II, and this means that the disc wear is mild and there is lubricant in the contact between the HSS pin and the steel 445 in this second stage, and the wear depth of the disc does not increase after Stage I.

Fig. 5 shows the COF and HSS pin displacement as a function of sliding time for the pre-oxidised discs siding against HSS pins at 850 and 950 °C. The thickness of the oxide scale on pre-oxidised discs is 6.1±0.23 μm (Section 3.1). In this case, the initial contact was considered as metallic pin on oxidised disc.

The curves of COF, as shown in Fig.5a, are steady from the beginning to the end of the tests. The COF is smaller at 950 °C. Fig. 5b shows the pin displacement curves during the test. The displacements of the pins have a similar tendency to increase at the early stage and then to keep stable quickly. This means that the disc wear is uniform. The depth of the wear track at 950 °C is higher than that at 850 °C.

Fig. 6 shows the comparison of COFs for the HSS pins sliding against ferrtic stainless steel with or without oxide scale at 850 and 950 °C. Oxide scale on the steel 445 plays a significant role in reducing COFs and in increasing stabilization at the first stage at elevated temperature. At the higher temperature of 950 °C, the COF and the standard deviations are smaller. For the clean discs in Stage II, the COF is less than 1/3 of that in Stage I. It can be concluded that the tribological behaviour of the contact has changed in Stage II.

Fig. 7 presents the macro-worn surfaces of HSS pins and corresponding discs tested at 850 and 950 °C. Normally, oxides on the surface of Fe-based metal will change the colour of the base metal after a wear test [30]. For instance, $Fe_2O_3$ appears in red and $Fe_3O_4$ in black, while the base metal displays a metallic luster. From Fig. 7a-d, the difference between the colours and worn areas of pins can be seen. Fig.7a and c show the worn surfaces of the HSS pins after sliding against clean discs. The surfaces appeared uneven but the worn surfaces were relatively smooth and partially blackened. The pin surface had a larger metallic shiny area at 850 °C than at 950 °C. Fig. 7b and d show the worn surfaces of the HSS pins after sliding against pre-oxidised discs. The surfaces appeared even and displayed some signs of rubbing. The shiny surface, as shown in

Fig.7b, is on the pin surface at 850 °C. Apart from this, the surfaces were covered with black oxides. Fig.7a1-d1 shows the wear track of the discs. The wear looks rough and severe for the clean discs, and the wear track width appears wider at 950 °C. The wear on the pre-oxidised discs, as seen in Fig. 7b1 and d1, is very mild. The colour of the track was only paler than the black oxidised surface and no metallic colour was observed.

Fig. 8 shows SEM micrographs of the worn surface of the HSS pins on clean discs at 850 and 950 °C, respectively. The surfaces were covered with the ferritic stainless steel transferred from the discs. EDS spectra of the black part on the HSS surface show that they are Fe,Cr oxides.

Fig. 9 shows SEM micrographs of the worn surface of the ferritic stainless steel 445 discs at 850 and 950 °C, respectively. The disc tracks have been cleaned by high pressure compressive air, so that any loose debris could be removed. The worn surface in the wear track seems to have a similar appearance. There was delamination of the ferritic stainless steel. EDS spectra of the worn surface in the wear track of the steel 445 discs show the oxides with Fe, Cr as the main constituent generated during the test. The oxides have been compacted and sintered in the wear track.

Black wear debris particles were generated on the clean discs. Most wear debris particles were transferred to the disc surface. A small amount of the wear debris particles remained in the contact zone. There were more wear debris particles on the disc tested at 950 °C, and they were

collected and ground to powder for XRD analysis. Fig. 10 shows that the wear debris generated on the clean disc is mainly $Cr_2O_3$ and there is a small amount of stainless steel substrate.

Fig. 11 shows SEM micrographs of the worn surface of the HSS pins on the pre-oxidised discs at 850 and 950 °C, respectively. Fig. 11a shows the zone that appears bright on the worn surface of the HSS pin at 850 °C. Slight scratch marks were observed on the worn surface, indicating abrasive wear. EDS spectrum 2 shows that the wear particles in an irregular shape are Cr-rich oxides. For the worn surface of the HSS pin at 950 °C, as shown in Fig.11b, the Cr-rich oxides are prevalent on the surface, as indicated by EDS spectrum 4. The Cr-rich oxides were transferred from the pre-oxidised discs on which the oxide scale was mainly made of $Cr_2O_3$.

Fig. 12 shows SEM micrographs of the worn surface of pre-oxidised ferritic stainless steel 445 discs at 850 and 950 °C, respectively. The worn surface in the wear track has a similar appearance. The worn surface was filled with powder-like particles and somewhere in the wear track the powder was compacted. EDS spectra 1 and 2 show that the particles contain mainly Cr and O. There is Fe at both temperatures, and most of that is from the iron oxides on the HSS pins. It indicates that the oxide scale on the steel 445 was broken into small particles. Some unbroken spinels still appeared on the worn surface but they were pressed into the powder- like oxides.

Fig. 13a and b show the cross-sections of the wear tracks on the clean discs. The oxides generated during the test (Fig. 10) compacted and mingled with the stainless steel substrate. Fig. 13c and d show the cross-section of the worn tracks on the pre-oxidised discs. They were very similar between 850 and 950 °C. Checking the whole cross-section of worn tracks, no through thickness cracks were observed.

## 4. Discussion

Fig. 14a shows the worn surfaces of the HSS pin and the corresponding disc-worn track after an interrupted pin-on-disc test at 850 °C, which was terminated after 480 sec in Stage I. The COF fluctuated severely during this Stage (Fig. 4). The worn surface of the HSS pin is different from that in Fig. 7a which was presented at the end of Stage II. The worn surface of the pin is very rough, as seen in the 3-D surface feature. The wear of the disc is also different from that at the end of Stage II (Fig. 7a1). There were no obvious black wear particles in the worn track or on the surface. The worn surface of the disc appeared metallic colour. This indicates that the oxide debris generated in Stage II played a significant role in reducing and in stabilizing the values of COF. The COF curve is different from carbon steels on which the oxide scale will form to a thickness of 75 μm at 900 °C in 2 mins [31]; therefore the setting of initial contact of high temperature pin-on-disc must be metal-oxide or oxide-oxide contact [25,32]. The oxidation rate of carbon steels increases considerably at or above 570 °C, due to establishment of a rapidly growing non-stoichiometric FeO formed at the metal/oxide interface [26]. In our experiment, this stainless steel 445 had very high resistance to oxidation at high temperature [5]; therefore the

initial contact of pin-to-disc was metal-metal contact. The disc substrate of steel 445 became soft at elevated temperature, while HSS was much harder. In Stage I, the soft stainless steel was ploughed by the harder HSS pin, therefore the steel 445 discs underwent severe abrasive wear. It also showed a strong adhesive bond between the high speed steel and the ferritic stainless steel 445, because the steel 445 was transferred and bonded to the HSS pin at high temperature. The contact surface became rougher and the adhesive wear became severe between the same materials at the point of contact (Fig. 14a), and this caused severe fluctuation of COFs in Stage I. The decrease in COF in Stage I (Fig. 4) should be related to the formation of oxide debris in this stage although the amount of oxide was limited but generated more over time. In Stage II, the metal debris in Stage I of sliding and the subsequent fracture exposed the fresh metal to further oxidation under frictional heating and high temperature [33]. $Cr_2O_3$ started to form abundantly (Fig. 10), and the newly generated particles started agglomerating in certain locations, particularly in the grooves of the pins and discs, and this became load-bearing and prevented metal-metal contact [34]. The wear debris was also mixed together with the steel substrate (Fig.13a and b), and a harder surface on the substrate was formed because $Cr_2O_3$ is a hard ceramic particle [35] and can enhance the hardness of the sliding surface [36]. In the presence of high compressive pressures of the wear tests, sintering is enhanced [37,38]. On the other hand, the surfaces of the HSS pins were partially oxidised (Fig. 8a and b) during rubbing the wear particles, and the patchy black area is considered to be wear-protective tribofilms [38,39]. This process was facilitated by the higher temperature (Fig. 4) and the value of COF levelled at 950 °C in a shorter time than that at 850 °C.

The oxide scale on the ferritic stainless steel, mainly $Cr_2O_3$, is harder than HSS at room temperature [23]. The HSS showed abrasive marks at 850 °C (Fig. 11a) but not at 950 °C, indicating that the hardness of the oxide scale decreased with increasing temperature. The oxide scale also showed good ductility without displaying any through thickness fracture (Fig. 13c and d) at both temperatures. The irregular spinels (Fig. 2a), either broken into particles or pressed into the oxide scale (Fig. 12a and b), did not show different tribological behaviour at the two different temperatures. The oxide scale developed on the HSS pin when metal - oxide contact took place in 15 mins at 950 °C [25], and this helped to reduce the COF at the early stage. The dropping of COF from 0.3 to 0.26 at 950 °C during the first 1 min may be attributed to this oxide-oxide contact. The surfaces of HSS pins showed Cr-rich oxide particles transferred from the pre-oxidised discs (Fig. 11a and b). This Cr-rich oxide can inhibit the growth of iron oxides on the surface of the HSS [26,8,5]. On the other hand, the $Cr_2O_3$ oxide debris was pressed and sintered on the surface of the HSS pin and formed a glaze layer (Fig. 11a and b), which is beneficial for reducing friction and wear [40,9,41-43]

Fig. 14b shows the worn surfaces of the HSS pin and the corresponding disc-worn track of the pin on pre-oxidised disc under a load of 70 N at 950 °C. In fact, this test was automatically terminated at 4 secs due to heavy fluctuation of the frictional force which had exceeded the maximum limitation of 200 N. Breakdown of the oxide scale on the steel 445 disc was observed, and the wear track of the disc showed a metallic colour and some black wear particles, definitely $Cr_2O_3$, were located in the worn track and on the surface of the disc. The disc material was transferred to the pin surface because there was no protection against metal-to-metal contact because of the breakdown of the oxide scale on the disc surface. The wear mechanism under

such a high load would similar to the frictional condition of the pin on the clean disc. Stott et al. [43] have investigated the breakdown of wear-protective oxide 'glaze' layers which depend on the load and the substrate hardness but it should be noted that oxide scale on the pre-oxidised disc is not a 'glaze' layer from the compaction of wear particle debris.

Fig. 15 illustrates the wear mechanism at elevated temperature when the HSS pin encountered the ferritic stainless steel 445 with or without oxide scale in dry sliding test. The oxide of $Cr_2O_3$, no matter in what forms, affected the wear and the frictional condition at high temperature. It would be beneficial to promote formation of the Cr-rich oxides on such a ferritic stainless steel in hot working conditions.

## 5. Conclusions

Tribological tests were carried out under a pin-on-disc configuration on a CETR tribometer at 850 and 950 °C in air.

At high temperature, the Cr-rich oxide scale on the steel 445 played a major role in friction and wear. Without the oxide scale on the steel 445, in the early stage, the COF fluctuated and the pin showed adhesive wear accumulated material transferred from the steel 445, indicating that there is a strong metallic bond between the HSS and the steel 445 at high temperature. As the temperature increased, the time needed for severe-mild wear transition decreased. The mild wear in the second stage was caused by the formation of oxides of $Cr_2O_3$ wear particles.

The Cr-rich Oxide scale on the steel 445 is very beneficial for preventing metal-metal contact and thus reducing friction. The wear of the HSS pin and the value of the COF were the minimum at 950 °C when there was oxide scale on the steel 445. Abrasive wear of the HSS pin was observed at 850 °C, indicating that the hardness of the oxide scale increased as temperature decreased.

The oxide scale with $Cr_2O_3$ as its main constituent, although it is harder than HSS at room temperature, showed ductility, prevented adhesive wear, and stabilized COF at high temperature. The $Cr_2O_3$ particles generated during the pin-on-clean-disc tests played a significant role in changing the wear and frictional behaviour. It outperformed the oxidation of the HSS pin in the experiment.

## Acknowledgements

The authors acknowledge the Baosteel-Australia Joint Research and Development Centre financial support for the current project under Grant number BA11017. The authors would like to also acknowledge engineers from Baosteel, Jianguo Peng, Ming Luo, Li Ma and Wei Du, to collaborate with the project. The authors wish to gratefully acknowledge the help of Dr. Madeleine Strong Cincotta in the language editing of this paper.

## References

1. Krzyzanowski, M., Beynon, J.H., Farrugia, D.C.J.: Oxide Scale Behavior in High Temperature Metal Processing, 1 ed. Wiley, Hoboken (2010)
2. Hidaka, Y., Anraku, T., Otsuka, N.: Deformation of Iron Oxides upon Tensile Tests at 600–1250°C. Oxid. Met. **59**(1-2), 97-113 (2003). doi:10.1023/a:1023070016230
3. Peckner, D., Bernstein, I.M.: Handbook of stainless steels. McGraw-Hill Book Company, New York (1977)
4. Reichardt, M.: Surface oxide formation and acid-descaling for stainless steel. Wire Ind. **68**, 503, 505-507 (2001).
5. Cheng, X., Jiang, Z., Wei, D., Zhao, J., Monaghan, B.J., Longbottom, R.J., Jiang, L.: Characteristics of oxide scale formed on ferritic stainless steels in simulated reheating atmosphere. Surf. Coat. Technol. **258**, 257-267 (2014). doi:10.1016/j.surfcoat.2014.09.019
6. Cheng, X., Jiang, Z., Wei, D., Zhao, J., Monaghan, B.J., Longbottom, R.J., Jiang, L.: High temperature oxidation behaviour of ferritic stainless steel SUS 430 in humid air. Met. Mater. Int. **21**(2), 251-259 (2015). doi:10.1007/s12540-015-4168-5
7. Cheng, X., Jiang, Z., Wei, D.: Effects of oxide scale on hot rolling of an austenitic stainless steel. Int. J. Surface Science and Engineering **8**(2-3), 173-187 (2014). doi:10.1605/01.301-0026661696.2014
8. Young, D.J.: High Temperature Oxidation And Corrosion Of Metals. Elsevier, Oxford (2008)
9. Stott, F.H.: High-temperature sliding wear of metals. Tribol. Int. **35**(8), 489-495 (2002). doi:10.1016/S0301-679X(02)00041-5
10. Fontalvo, G.A., Mitterer, C.: The effect of oxide-forming alloying elements on the high temperature wear of a hot work steel. Wear **258**(10), 1491-1499 (2005). doi:10.1016/j.wear.2004.04.014
11. Masuko, M., Iijima, S., Terawaki, T., Suzuki, A., Aoki, S., Nogi, T., Obara, S.: Effect of Surface Oxide Layer of Steel on the Tribological Characteristics of Load-bearing Additives for Multiply-Alkylated Cyclopentane Oil under High Vacuum. Tribol. Lett. **51**(1), 115-125 (2013). doi:10.1007/s11249-013-0152-8
12. Lundberg, S.-E., Gustafsson, T.: The influence of rolling temperature on roll wear, investigated in a new high temperature test rig. J. Mater. Process Tech. **42**(3), 239-291 (1994). doi:10.1016/0924-0136(94)90181-3
13. Stott, F.H.: The role of oxidation in the wear of alloys. Tribol. Int. **31**(1-3), 61-71 (1998). doi:10.1016/s0301-679x(98)00008-5
14. Kato, H.: Effects of supply of fine oxide particles onto rubbing steel surfaces on severe-mild wear transition and oxide film formation. Tribol. Int. **41**(8), 735-742 (2008). doi:10.1016/j.triboint.2008.01.001
15. Hai, W., Zeng, J., Zhang, R., Meng, J., Lu, J.: Oxide-based tribofilms and tribological behavior of self-mated Ti3SiC2 lubricated by PbO powders at high temperatures in nitrogen flow. Wear **317**(1-2), 233-240 (2014). doi:10.1016/j.wear.2014.05.018
16. Iwabuchi, A., Hori, K., Kubosawa, H.: The effect of oxide particles supplied at the interface before sliding on the severe-mild wear transition. Wear **128**(2), 123-137 (1988). doi:10.1016/0043-1648(88)90179-2
17. Hiratsuka, K., Inagaki, M.: Effects of temperature, sliding velocity and non-friction time on severe-mild wear transition of iron. Tribol. Int. **49**, 39-43 (2012). doi:10.1016/j.triboint.2011.12.004

18. Hiratsuka, K.i., Muramoto, K.i.: Role of wear particles in severe–mild wear transition. Wear **259**(1–6), 467-476 (2005). doi:10.1016/j.wear.2005.02.102
19. Battez, A.H., Gonzalez, R., Felgueroso, D., Fernandez, J.E., Fernandez, M.D., Garcia, M.A., Penuelas, I.: Wear prevention behaviour of nanoparticle suspension under extreme pressure conditions. Wear **263**, 1568-1574 (2007). doi:10.1016/j.wear.2007.01.093
20. Ha, D.J., Sung, H.K., Lee, S., Lee, J.S., Lee, Y.D.: Analysis and prevention of sticking occurring during hot rolling of ferritic stainless steel. Mater. Sci. Eng., A **507**(1–2), 66-73 (2009). doi:10.1016/j.msea.2008.11.062
21. Jin, W., Choi, J.Y., Lee, Y.Y.: Effect of roll and rolling temperatures on sticking behavior of ferritic stainless steels. ISIJ Int. **38**(7), 739-743 (1998). doi:10.2355/isijinternational.38.739
22. Hao, L., Jiang, Z., Cheng, X., Zhao, J., Wei, D., Jiang, L., Luo, S., Luo, M., Ma, L.: Effect of Extreme Pressure Additives on the Deformation Behavior of Oxide Scale during the Hot Rolling of Ferritic Stainless Steel Strips. Tribol. T. **58**(5), 947-954 (2015). doi:10.1080/10402004.2015.1025931
23. Cheng, X., Jiang, Z., Zhao, J., Wei, D., Hao, L., Peng, J., Luo, M., Ma, L., Luo, S., Jiang, L.: Investigation of oxide scale on ferritic stainless steel B445J1M and its tribological effect in hot rolling. Wear **338–339**, 178-188 (2015). doi:10.1016/j.wear.2015.06.014
24. Cheng, X., Jiang, Z., Wei, D., Hao, L., Zhao, J., Jiang, L.: Oxide scale characterization of ferritic stainless steel and its deformation and friction in hot rolling. Tribol. Int. **84**(0), 61-70 (2015). doi:10.1016/j.triboint.2014.11.026
25. Vergne, C., Boher, C., Levaillant, C., Gras, R.: Analysis of the friction and wear behavior of hot work tool scale: application to the hot rolling process. Wear **250**, 322-333 (2001). doi:10.1016/s0043-1648(01)00598-1
26. Birks, N., Meier, G.H., Pettit, F.S.: High-Temperature Oxidation of Metals, 2nd ed. Cambridge University Press, Cambridge (2005)
27. Cheng, X., Jiang, Z., Monaghan, B.J., Wei, D., Longbottom, R.J., Zhao, J., Peng, J., Luo, M., Ma, L., Luo, S., Jiang, L.: Breakaway oxidation behaviour of ferritic stainless steels at 1150°C in humid air. Corr. Sci. **108**, 11-22 (2016). doi:10.1016/j.corsci.2016.02.042
28. Stott, F.H., Wei, F.I., Enahoro, C.A.: The influence of manganese on the High-temperature oxidation of iron-chromium alloys. Mater. Corros. **40**(4), 198-205 (1989). doi:10.1002/maco.19890400403
29. Meier, G.H., Jung, K., Mu, N., Yanar, N.M., Pettit, F.S., Abellan, J.P., Olszewski, T., Hierro, L.N., Quadakkers, W.J., Holcomb, G.R.: Effect of Alloy Composition and Exposure Conditions on the Selective Oxidation Behavior of Ferritic Fe–Cr and Fe–Cr–X Alloys. Oxid. Met. **74**(5-6), 319-340 (2010). doi:10.1007/s11085-010-9215-5
30. Zhu, Y., Olofsson, U., Chen, H.: Friction Between Wheel and Rail: A Pin-On-Disc Study of Environmental Conditions and Iron Oxides. Tribol. Lett. **52**(2), 327-339 (2013). doi:10.1007/s11249-013-0220-0
31. Chen, R., Yuen, W.Y.D.: Short-time Oxidation Behavior of Low-carbon, Low-silicon Steel in Air at 850–1,180 °C—I: Oxidation Kinetics. Oxid. Met. **70**(1-2), 39-68 (2008). doi:10.1007/s11085-008-9111-4
32. Vergne, C., Boher, C., Gras, R., Levaillant, C.: Influence of oxides on friction in hot rolling: Experimental investigations and tribological modelling. Wear **260**(9-10), 957-975 (2006). doi:10.1016/j.wear.2005.06.005

33. Stott, F.H., Wood, G.C.: Influence of oxides on friction and wear of alloys. Tribol. Int. **11**(4), 211-218 (1978). doi:10.1016/0301-679x(78)90178-0
34. Jiang, J.R., Stott, F.H., Stack, M.M.: Some frictional features associated with the sliding wear of the nickel-base alloy N80A at temperatures to 250 °C. Wear **176**(2), 185-194 (1994). doi:10.1016/0043-1648(94)90146-5
35. Pelleg, J.: Mechanical Properties of Ceramics. Springer, (2014)
36. Rynio, C., Hattendorf, H., Klöwer, J., Eggeler, G.: On the physical nature of tribolayers and wear debris after sliding wear in a superalloy/steel tribosystem at 25 and 300°C. Wear **317**(1-2), 26-38 (2014). doi:10.1016/j.wear.2014.04.022
37. Pauschitz, A., Roy, M., Franek, F.: Mechanisms of sliding wear of metals and alloys at elevated temperatures. Tribol. Int. **41**, 584-602 (2008). doi:10.1016/j.triboint.2007.10.003
38. Kato, H., Komai, K.: Tribofilm formation and mild wear by tribo-sintering of nanometer-sized oxide particles on rubbing steel surfaces. Wear **262**(1-2), 36-41 (2007). doi:10.1016/j.wear.2006.03.046
39. Han, J.S., Jia, J.H., Lu, J.J., Wang, J.B.: High Temperature Tribological Characteristics of Fe-Mo-based Self-Lubricating Composites. Tribol. Lett. **34**(3), 193-200 (2009). doi:10.1007/s11249-009-9423-9
40. Blau, P.J., Brummett, T.M.: High-Temperature Oxide Regrowth on Mechanically Damaged Surfaces. Tribol. Lett. **32**(3), 153-157 (2008). doi:10.1007/s11249-008-9372-8
41. Stott, F.H., Glascott, J., Wood, G.C.: Factors affecting the progressive development of wear-protective oxides on iron-base alloys during sliding at elevated-temperatures. Wear **97**(1), 93-106 (1984). doi:10.1016/0043-1648(84)90084-x
42. Stott, F.H., Glascott, J., Wood, G.C.: The sliding wear of commercial Fe-12%Cr alloys at high temperature. Wear **101**(4), 311-324 (1985). doi:10.1016/0043-1648(85)90135-8
43. Stott, F.H., Jordan, M.P.: The effects of load and substrate hardness on the development and maintenance of wear-protective layers during sliding at elevated temperatures. Wear **250**, 391-400 (2001). doi:10.1016/s0043-1648(01)00601-9

**Table Captions:**

**Table 1** Chemical composition (wt. %) of the high speed steel, pin material.

**Table 2** Chemical composition (wt. %) of the ferritic stainless steel 445, disc material.

**Figure Captions:**

**Fig. 1** Schematic illustration of high temperature pin-on-disc test configuration.

**Fig. 2** Surface features of the steel 445oxidised at 1100 ºC for 120 min: (a) micrograph of the surface of the oxide scale, (b) XRD pattern of the oxide scale, and (c) cross section of the oxide scale.

**Fig. 3** Rockwell hardness indents (a) clean disc and (b) oxidised disc.

**Fig. 4** HSS pins sliding against clean ferritic stainless steel discs at 850 and 950 °C. (a) Coefficient of friction, and (b) pin displacement as a function of sliding time.

**Fig. 5** HSS pins sliding against pre-oxidised ferritic stainless steel discs at 850 and 950 °C. (a) Coefficient of friction, and (b) pin displacement as a function of sliding time.

**Fig. 6** Comparison of COF for the ferritic stainless steel with or without oxide scale at elevated temperatures.

**Fig. 7** Worn surfaces of pins and corresponding disc worn tracks after high temperature pin-on-disc test.

**Fig. 8** SEM and EDS analysis of worn surfaces of HSS pins on clean discs (a) 850 and (b) 950 °C.

**Fig. 9** SEM and EDS analysis of worn surfaces of clean discs (a) 850 and (b) 950 °C (the yellow arrows indicate sliding direction, and the green arrows indicate the delamination).

**Fig. 10** The XRD analysis of wear debris on clean disc.

**Fig. 11** SEM and EDS analysis of worn surfaces of HSS pins on pre-oxidised discs (a) 850 and (b) 950 °C.

**Fig. 12** SEM and EDS analysis of worn surfaces of pre-oxidised discs (a) 850 and (b) 950 °C.

**Fig. 13** The cross section of the disc worn tracks (a) clean disc, 850 °C; (b) clean disc, 950 °C; (c) pre-oxidised disc, 850 °C; and (d) pre-oxidised disc, 950 °C.

**Fig. 14** Worn surfaces of pins and corresponding disc worn tracks (a) on clean disc at 850 °C for 480 secs in stage I, and (b) on pre-oxidised disc under a load of 70 N at 950 °C (failure at 4 secs).

**Fig. 15** Schematic illustration of the wear mechanism at elevated temperatures (a) HSS pin on clean discs, and (b) HSS pin on pre-oxidised discs.

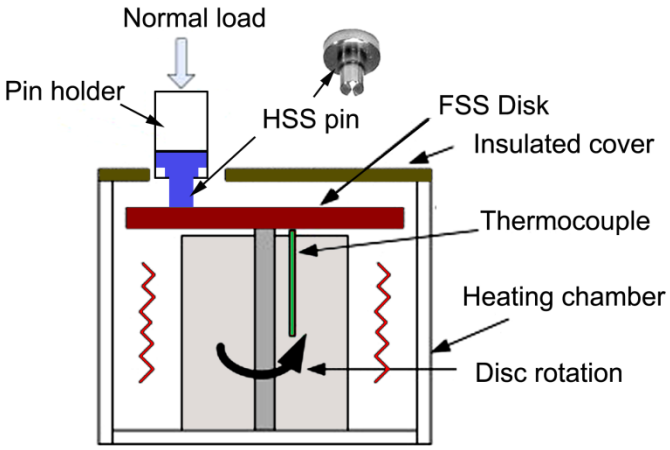


**Fig. 1** Schematic illustration of high temperature pin-on-disc test configuration

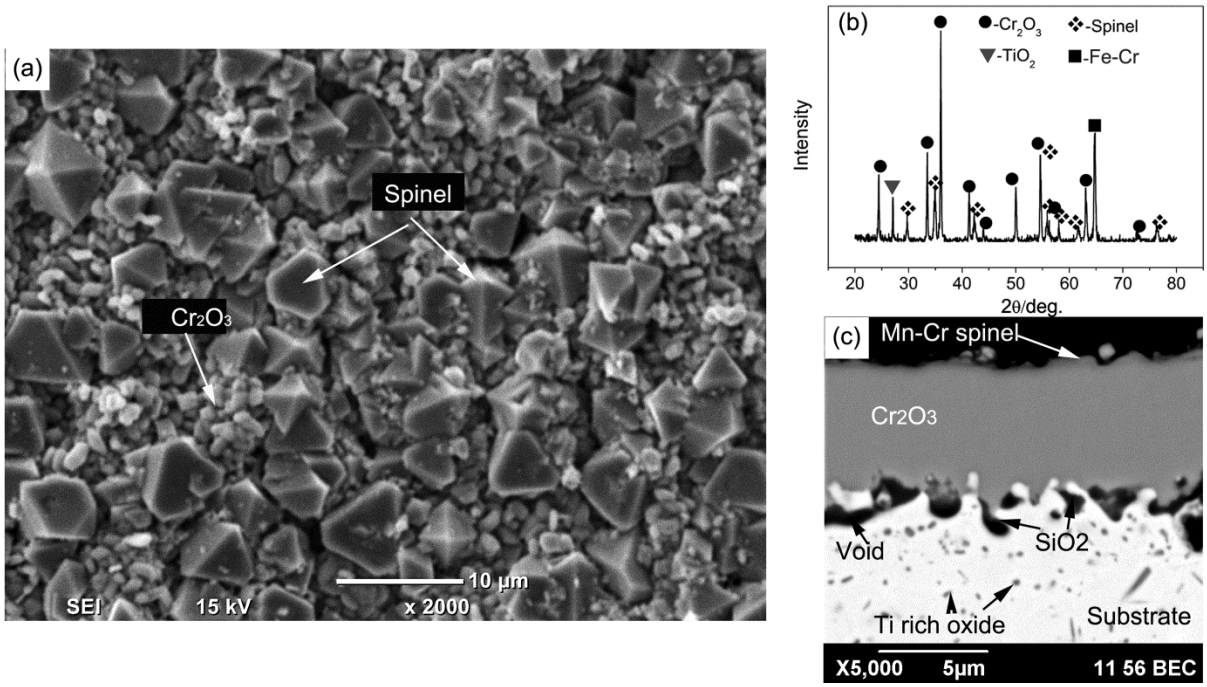


**Fig. 2** Surface features of the steel 445 oxidised at 1100 ºC for 120 min: (a) micrograph of the surface of the oxide scale, (b) XRD pattern of the oxide scale, and (c) cross section of the oxide scale

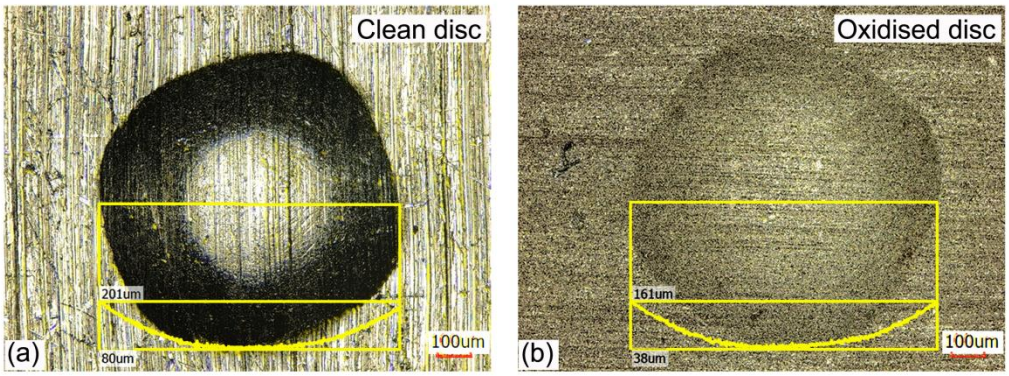


**Fig. 3** Rockwell hardness indents (a) clean disc and (b) oxidised disc

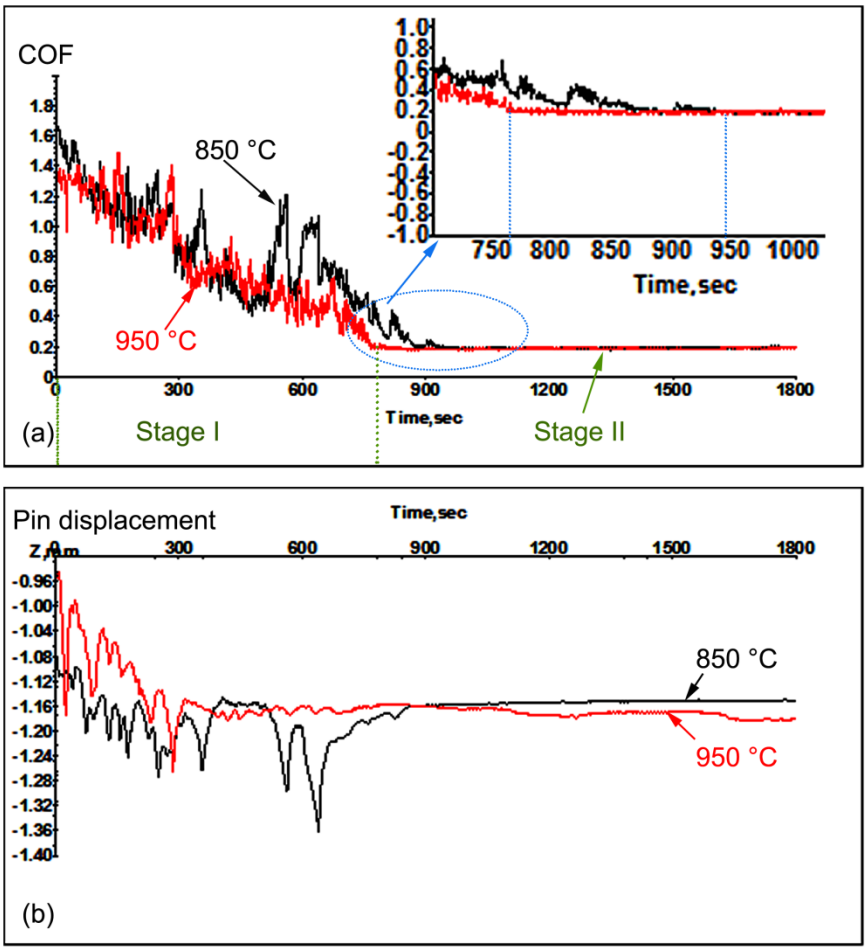


**Fig. 4** HSS pins sliding against clean ferritic stainless steel discs at 850 and 950 °C. (a) Coefficient of friction, and (b) pin displacement as a function of sliding time.

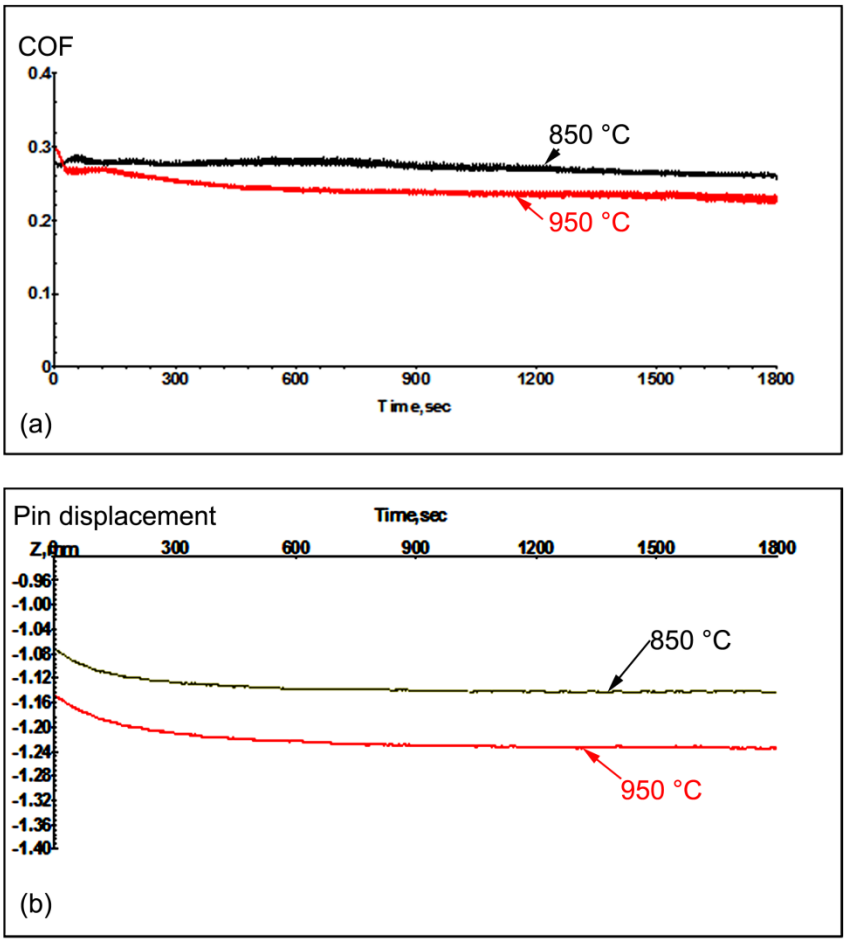


**Fig. 5** HSS pins sliding against pre-oxidised ferritic stainless steel discs at 850 and 950 °C. (a) Coefficient of friction, and (b) pin displacement as a function of sliding time.

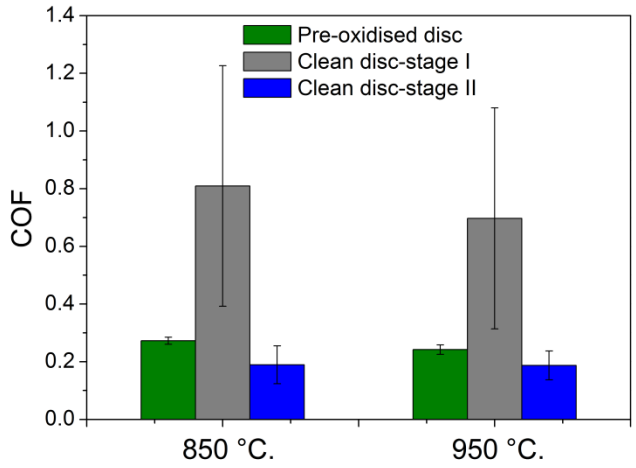


**Fig. 6** Comparison of COF for the ferritic stainless steel with or without oxide scale at elevated temperatures.

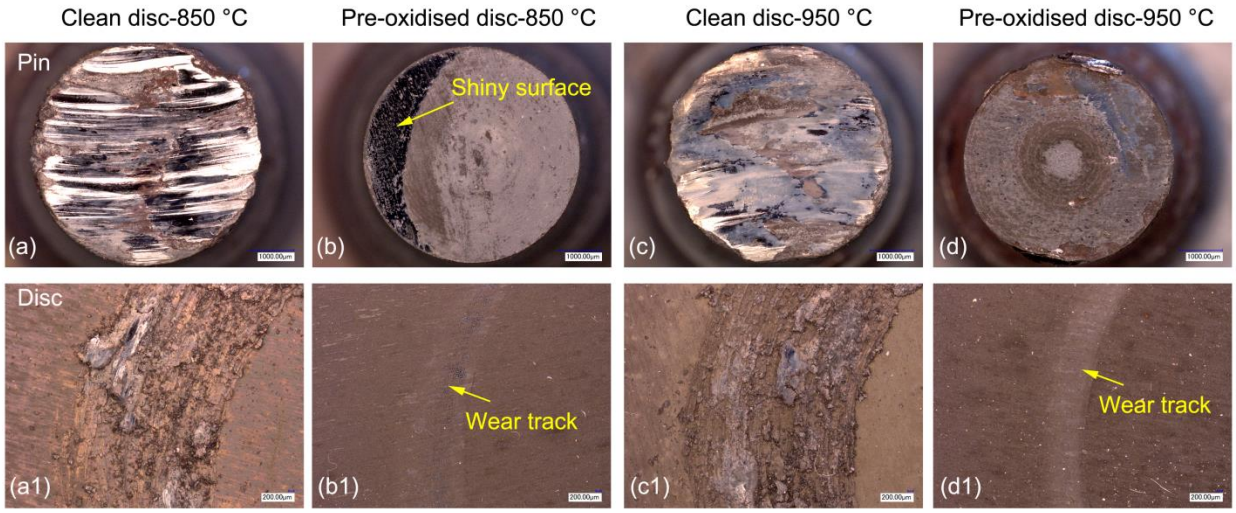


**Fig. 7** Worn surfaces of pins and corresponding disc worn tracks after high temperature pin-on-disc test.

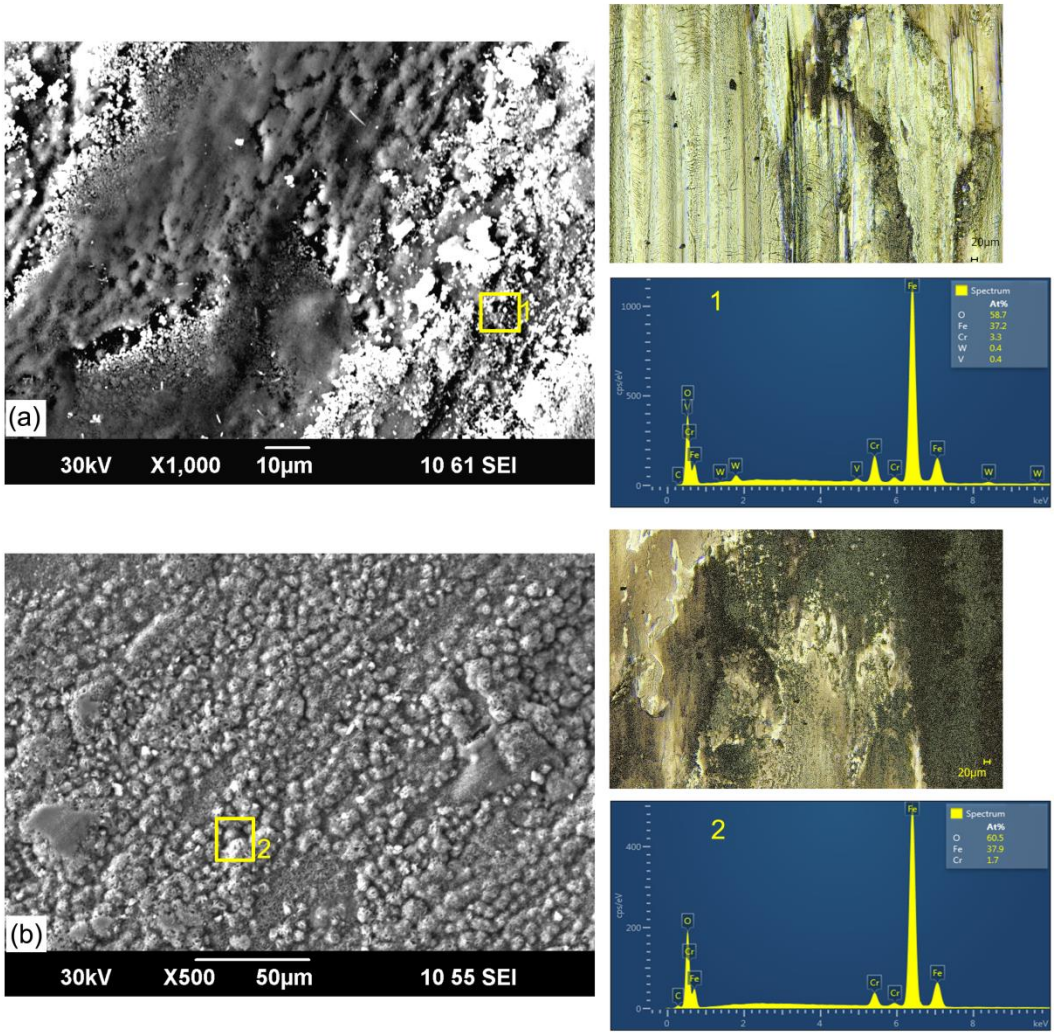


**Fig. 8** SEM and EDS analysis of worn surfaces of HSS pins on clean discs (a) 850 and (b) 950 °C.

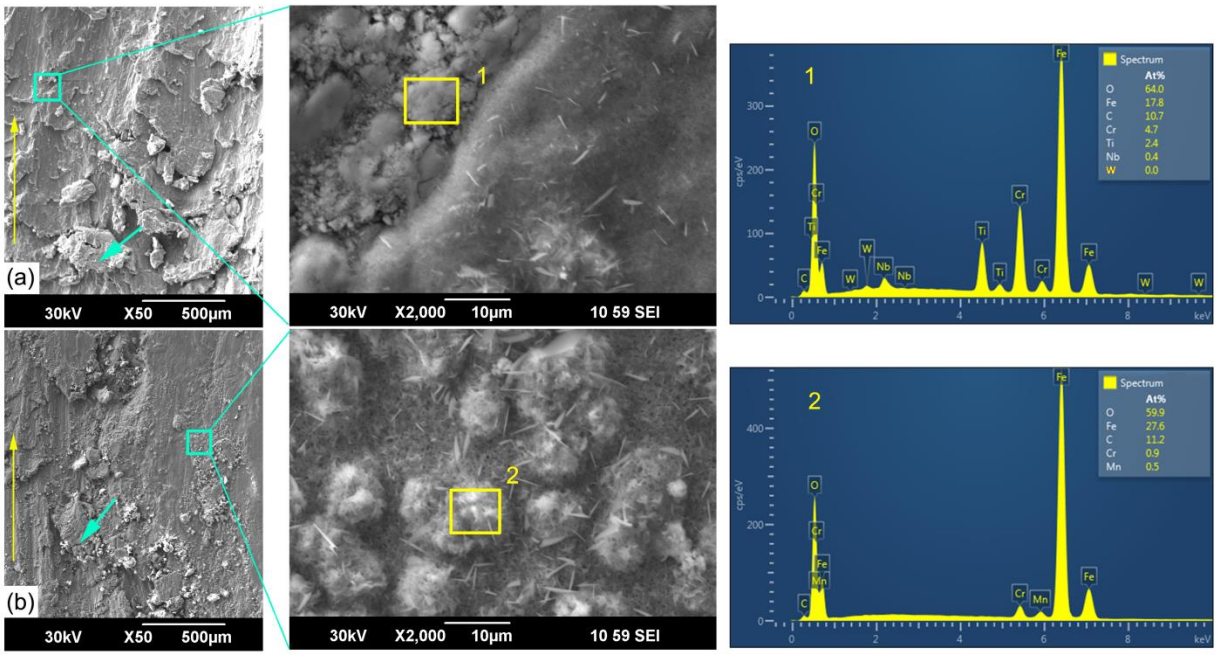


**Fig. 9** SEM and EDS analysis of worn surfaces of clean discs (a) 850 and (b) 950 °C (the yellow arrows indicate sliding direction, and the green arrows indicate the delamination).

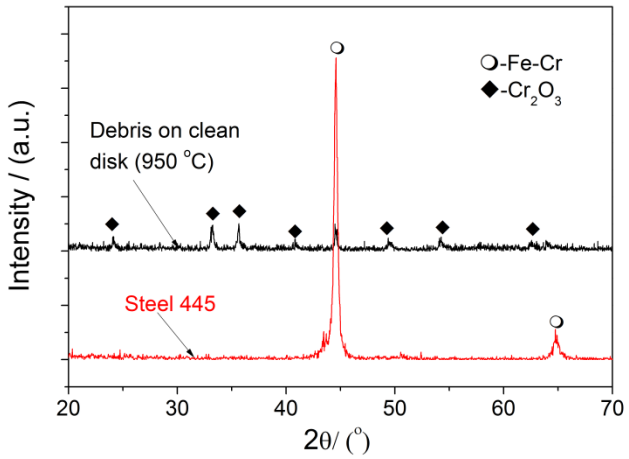


**Fig. 10** The XRD analysis of wear debris on clean disc

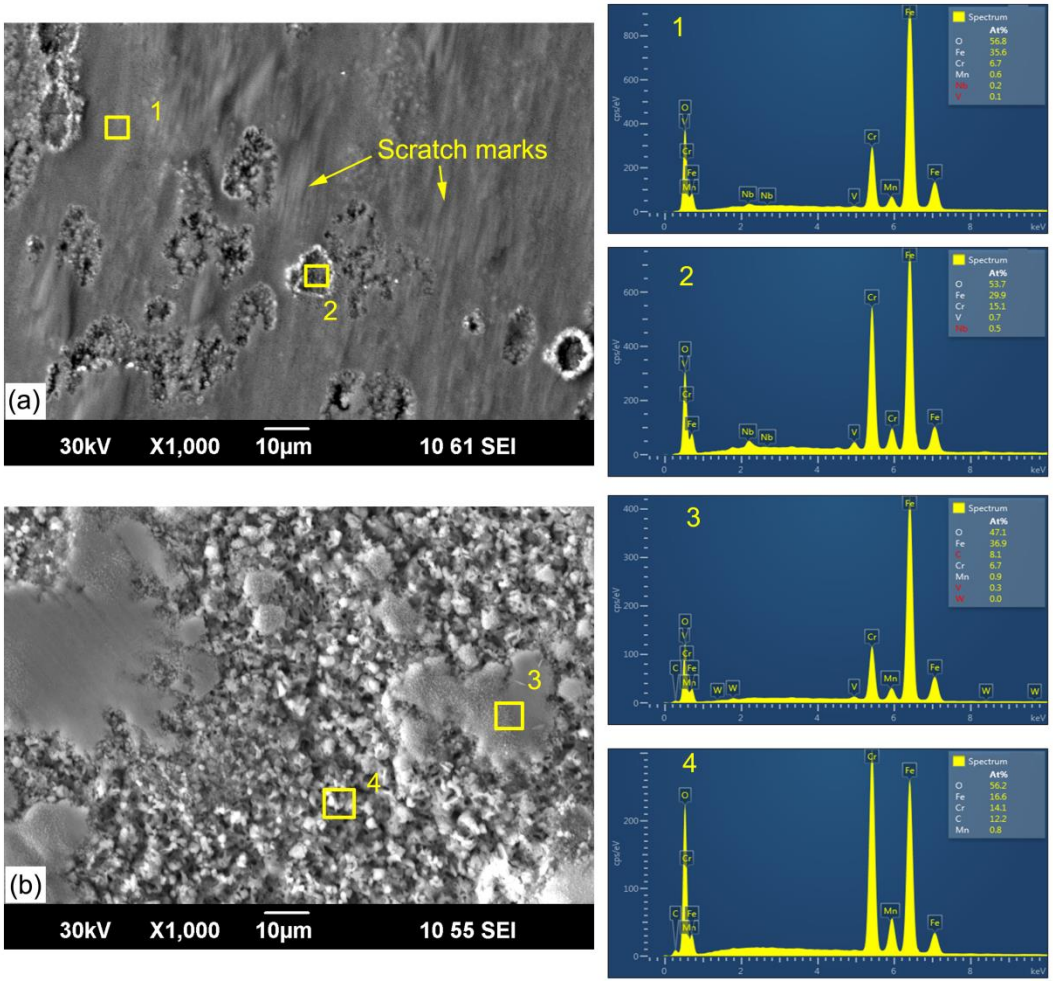


**Fig. 11** SEM and EDS analysis of worn surfaces of HSS pins on pre-oxidised discs (a) 850 and (b) 950 °C

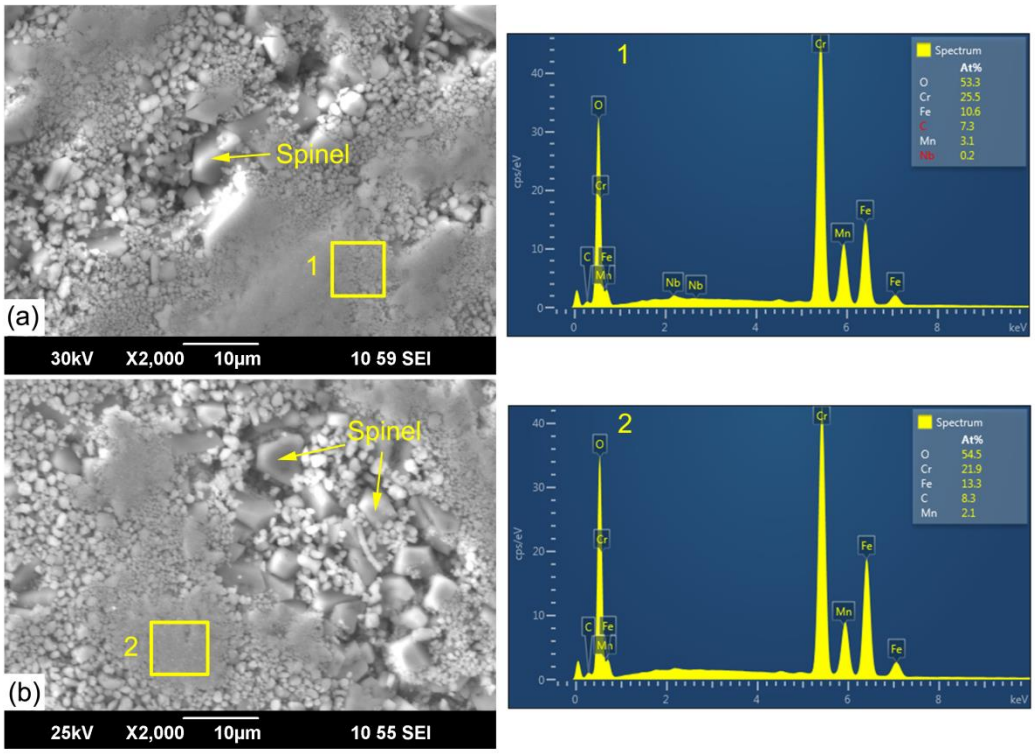


**Fig. 12** SEM and EDS analysis of worn surfaces of pre-oxidised discs (a) 850 and (b) 950 °C.

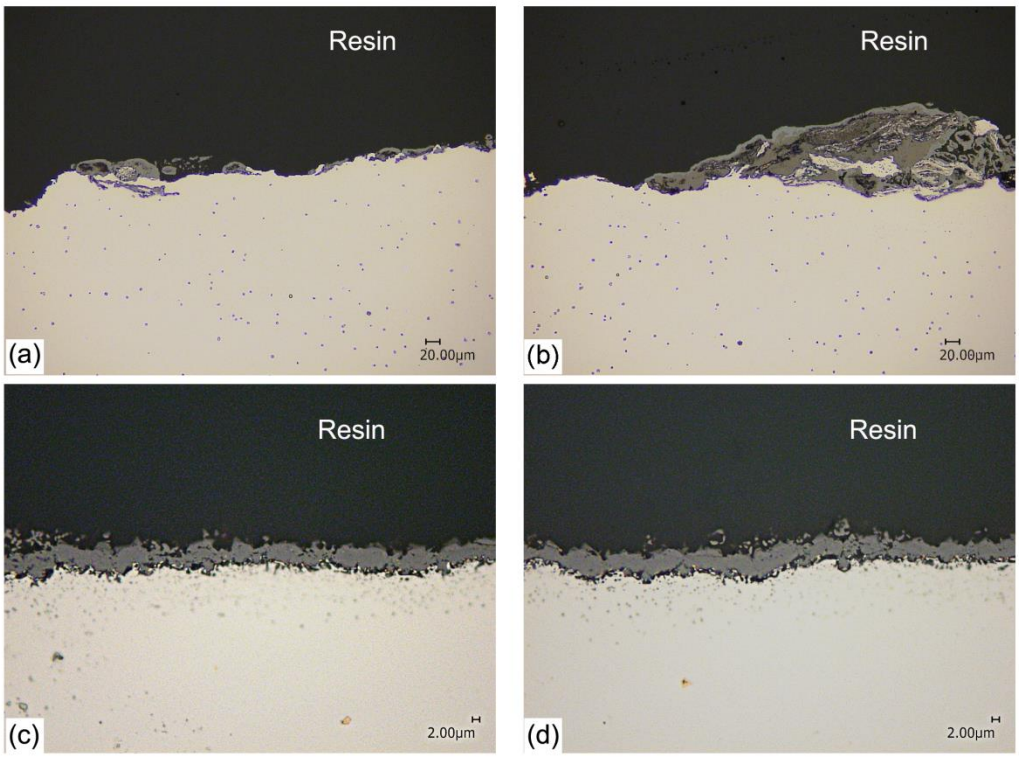


**Fig. 13** The cross section of the disc worn tracks (a) clean disc, 850 °C; (b) clean disc, 950 °C; (c) pre-oxidised disc, 850 °C; and (d) pre-oxidised disc, 950 °C.

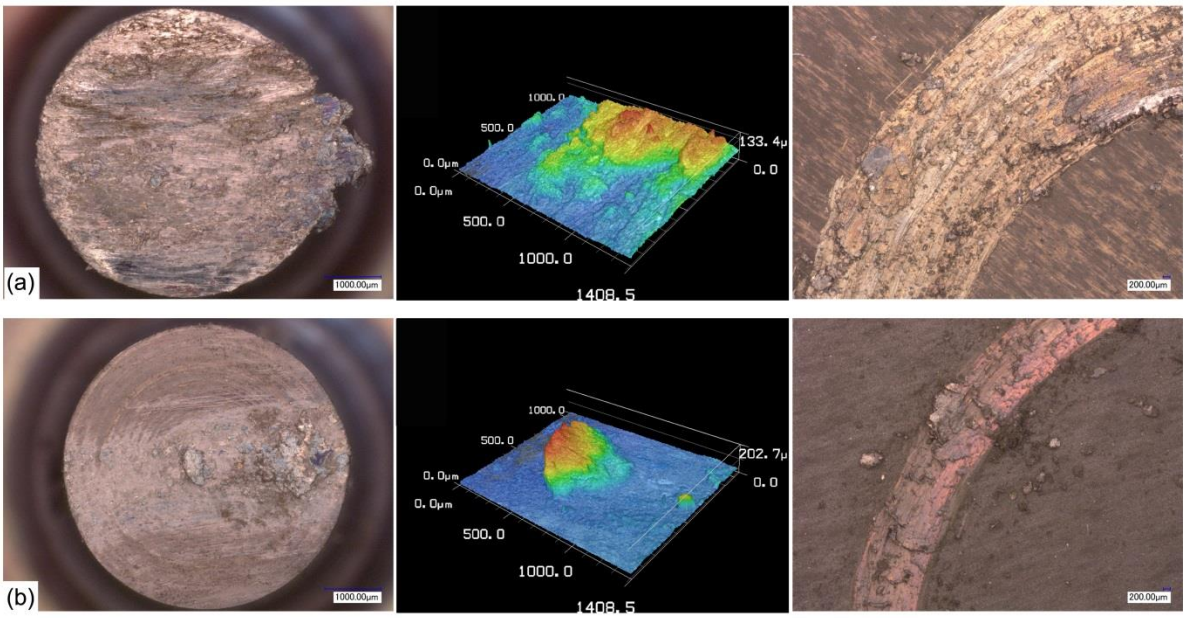


**Fig. 14** Worn surfaces of pins and corresponding disc worn tracks (a) on clean disc at 850 °C for 480 secs in stage I, and (b) on pre-oxidised disc under a load of 70 N at 950 °C (failure at 4 secs).

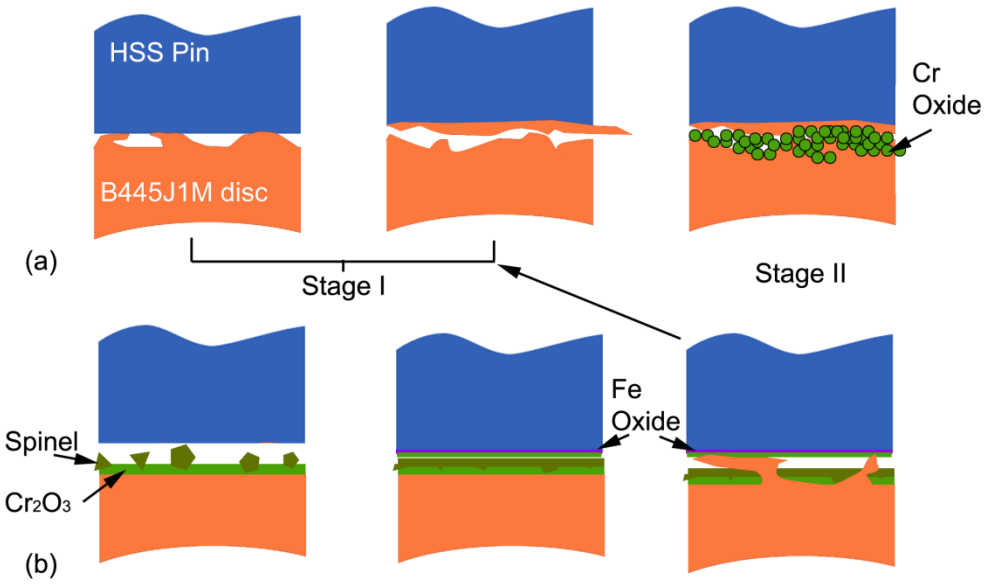


**Fig. 15** Schematic illustration of the wear mechanism at elevated temperatures (a) HSS pin on clean discs, and (b) HSS pin on pre-oxidised discs.

**Table 1** Chemical composition (wt. %) of the high speed steel, pin material.

| C | W | Mo | Cr | V | Sr | Mn | S | P | Impurities | Fe |
|---|---|---|---|---|---|---|---|---|---|---|
| 1.6 | 6.0 | 5.0 | 4.0 | 4.5 | 1.2 | 0.3 | 0.03 | 0.03 | <=0.1 | Bal |

**Table 2** Chemical composition (wt. %) of the ferritic stainless steel 445, disc material.

| C | Si | Mn | P | Cr | Cu | Mo | Ti | Nb | Fe |
|---|---|---|---|---|---|---|---|---|---|
| ≤0.01 | 0.30 | 0.15 | 0.03 | 21.50 | 0.10 | 0.60 | ≤0.20 | 0.12 | Bal |